Fig. 5

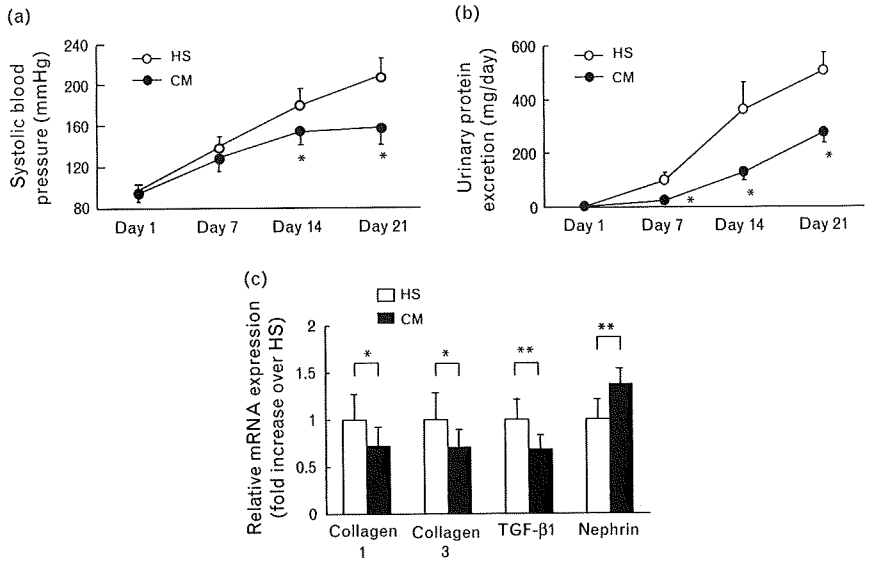

Effect of camostat mesilate on blood pressure, urinary protein excretion, and renal injury in Dahl salt-sensitive rats. SBP was measured by tail-cuff method at days 7, 14, and 21. Twenty-four-hour urinary collections were made in a metabolic cage, and urinary protein excretion was evaluated at each indicated day. Total RNA was extracted from kidneys of high salt and camostat mesilate rats at day 21. Real-time PCR analysis was performed for TGF-β1, collagen type I, collagen type III and nephrin. (a) Systolic blood pressure, (b) urinary protein excretion, and (c) renal injury markers. Results are expressed as mean ± SD ($n = 8$). CM, high-salt diet and camostat (0.1%); HS, high-salt diet; TGF-β1, transforming growth factor-β1. $^{*}P < 0.05$ vs. HS rats; $^{**}P < 0.01$ vs. HS rats; $^{***}P < 0.001$ vs. HS rats.

Camostat mesilate and FOY-251 decreased R_{te} as well as I_{eq} in M-1 cells. It has been demonstrated that aprotinin but not soybean trypsin inhibitor (STI) altered R_{te} of M-1 cells [23], indicating that protease activity affected the resistance of cultured epithelial cells. Because prostasin activity is sensitive to aprotinin but not to STI, the involvement of prostasin in the development of R_{te} is a strong possibility. Furthermore, Verghese *et al.* [24] revealed that overexpression of wild-type prostasin decreased R_{te} of M-1 cell monolayers, whereas overexpression of a protease-dead mutant of prostasin increased it. From these findings, it is considered that camostat mesilate and FOY-251 could alter R_{te} in epithelial cell monolayers by inhibiting prostasin activity.

Table 1 Physiological profiles of high salt and camostat mesilate rats

	HS	CM
Food consumption (g/day)	21.0 ± 1.4	20.6 ± 1.8
Sodium consumption (mmol/day)	28.6 ± 1.9	28.0 ± 2.5
Water consumption (ml/day)	145 ± 14	138 ± 12
Body weight (g)	237 ± 17	238 ± 8
Kidney weight (mg/g BW)	13.0 ± 0.6	10.8 ± 0.4*
Serum albumin (g/l)	28 ± 1	31 ± 1§
Serum creatinine (μmol/l)	32 ± 6	17 ± 1
Creatinine clearance (ml/min)	1.4 ± 0.4	2.4 ± 0.2*
Serum Na (mmol/l)	146 ± 1	145 ± 2
Serum K (mmol/l)	3.7 ± 0.4	3.8 ± 0.1
PRA (ng/l/s)	0.72 ± 0.17	0.89 ± 0.22
PAC (nmol/l)	46.3 ± 9.2	58.3 ± 21.1
Urine volume (ml/day)	118 ± 18	105 ± 16
Urinary Na excretion (mmol/day)	23.6 ± 6.9	27.8 ± 2.6
Urinary Na/K ratio	6.4 ± 0.6	7.0 ± 0.3#
Urinary camostat mesilate (μmol/l)	ND	ND
Urinary FOY-251 (μmol/l)	ND	10.51 ± 2.33

Data are expressed as mean ± SD ($n = 8$). CM, high-salt diet and camostat (0.1%) group; HS, high-salt diet group; ND, not detectable; PAC, plasma aldosterone content; PRA, plasma renin activity. $^{*}P < 0.001$ vs. HS group; $^{\S}P < 0.01$ vs. HS group; and $^{\#}P < 0.05$ vs. HS group.

In the present studies, we also investigated the antihypertensive and renoprotective effects of camostat mesilate on Dahl salt-sensitive rats fed with a high-salt diet. Our in-vitro data definitely demonstrated that both camostat mesilate and FOY-251 reduced ENaC activity, probably through the inhibition of prostasin activity. Therefore, we expected that administration of camostat mesilate would improve salt-sensitive hypertension, in which ENaC is exceedingly activated, and indeed, camostat mesilate substantially depressed SBP in Dahl salt-sensitive rats after 2 weeks of treatment. At day 21, sodium and water consumption, urine volume, and renal sodium excretion were not significantly different between Dahl salt-sensitive and camostat mesilate rats, but we observed a tendency toward natriuresis in camostat mesilate rats. The reason why renal sodium excretion was not increased with statistical significance in camostat mesilate rats may presumably be because the loading dose of sodium to Dahl salt-sensitive rats was too high to observe the effect of camostat mesilate on sodium balance. In other words, because an extremely large amount of sodium was filtered through the glomeruli and excreted into urine without tubular reabsorption because of the high-salt diet, small changes in sodium reabsorption caused by camostat

mesilate might not produce a statistically significant change in overall sodium excretion. However, we observed a statistically significant increase in the urinary Na/K ratio in camostat mesilate rats, which is widely used to evaluate aldosterone activity at the distal nephron and collecting duct [25]. Therefore, we believe that the elevation of the urinary Na/K ratio in camostat mesilate rats indicates the decrease in activity of ENaC. We determined the urinary concentrations of camostat mesilate and FOY-251 in camostat mesilate rats. As shown in Table 1, camostat mesilate was not detected in the urine of camostat mesilate rats, but the concentration of FOY-251 in the urine of camostat mesilate rats reached approximately 10 μmol/l. Considering that 10 μmol/l of FOY-251 sufficiently inhibited the activities of prostasin and ENaC *in vitro*, we believe that the dosage of camostat mesilate for our in-vivo experiments should be enough to suppress prostasin and ENaC in rat kidneys.

The Dahl salt-sensitive rat is a well known model of salt-sensitive hypertension; however, the mechanism by which the high-salt diet raises BP is not clearly defined. Aoi *et al.* [16] showed that high-salt diets increased the mRNA expression of α ENaC despite the presence of lower PAC levels in Dahl salt-sensitive rats. If the abnormal upregulation of ENaC actually contributes to the development of salt-sensitive hypertension in Dahl salt-sensitive rats, inhibitors of ENaC should ameliorate the hypertension. The antihypertensive effect of camostat mesilate demonstrated in our study would support their hypothesis that aberrant activation of ENaC under high-salt diet conditions is primarily responsible for the pathogenesis of salt-sensitive hypertension in Dahl salt-sensitive rats. In general, natriuresis should result in elevated PAC levels. However, we did not observe any change in PAC levels in camostat mesilate rats. A possible explanation for these conflicting results is that camostat mesilate may inhibit secretion of aldosterone by the adrenal gland. Tetsuo *et al.* [26] showed that intravenous infusion of nafamostat mesilate, a synthetic serine protease inhibitor, decreased aldosterone secretion from the adrenal gland in rats, although they did not determine the precise mechanism. Because camostat mesilate is structurally related to nafamostat mesilate, camostat mesilate has the potential to suppress the secretion of aldosterone *in vivo*. Further studies are required to elucidate this possibility.

Camostat mesilate rats displayed a decrease in both serum creatinine levels and urinary protein excretion, indicating a protective effect of camostat mesilate against kidney injury. TGF-β1 expression in the glomerulus, with the expansion of extracellular matrix, is elevated in various experimental renal diseases, including hypertension in Dahl salt-sensitive rats [27]. Treatment of Dahl salt-sensitive rats with camostat mesilate dramatically suppressed the high-salt diet-induced increase in TGF-β1, collagen type I, and collagen type III mRNA, and also ameliorated a decrease in nephrin expression. The alterations in mRNA expression of these genes have been clearly demonstrated to be associated with the severity of glomerular injury. These results strongly suggest that camostat mesilate had a beneficial effect on the kidney in Dahl salt-sensitive rats fed a high-salt diet. Significant reductions in BP in hypertensive animals and patients, of course, ameliorate injury to organs including the kidney, heart, brain, and vasculature. Thus, a simple explanation for the renoprotective effect of camostat mesilate on Dahl salt-sensitive rats comes from the marked decrease in BP. In addition, the association of high sodium intake and tissue injury has been extensively investigated in many experimental and clinical studies [28,29]. Elimination of salt by diuretics has been demonstrated to improve mortality and morbidity of hypertensive patients in a number of clinical trials [30]. Whether the renoprotective effects of camostat mesilate were solely a result of the substantial reduction in BP or from the natriuretic action or both remains to be determined. Several reports showed the effect of camostat mesilate on proteinuria in various nephropathies [31,32]. A hypercoagulable state with elevated plasma fibrinogen and impaired fibrinolysis has been reported to be involved in the progression of diabetic nephropathy [33]. Matsubara *et al.* [34] demonstrated that proteinuria in diabetic nephropathy was decreased through the inhibitory effect of camostat mesilate on the coagulation system and platelet function. They also showed that camostat mesilate decreased urinary protein excretion without changing BP in patients with advanced diabetic nephropathy [34]. Their findings suggest that camostat mesilate may have protective effects on the kidney apart from the reduction in BP, although we have not addressed this issue in the current investigation. According to the product document regarding camostat mesilate, camostat mesilate and FOY-251 have inhibitory effects on trypsin, plasmin, and plasma kallikrein with low 50% inhibitory concentration (approximately 1–100 nmol/l). Because the urinary concentration of FOY-251 is approximately 10 μmol/l as described above, these serine proteases could be inhibited by camostat mesilate in Dahl salt-sensitive rats. However, to our knowledge, there are no reports demonstrating a possible involvement of trypsin or plasmin in salt-sensitive hypertension. Although the inhibition of plasma kallikrein by camostat mesilate may affect BP through the kallikrein–kinin system, treatment with camostat mesilate theoretically should increase the BP. Therefore, we speculate that the contribution of trypsin, plasmin, and plasma kallikrein to the antihypertensive and natriuretic effects of camostat mesilate on Dahl salt-sensitive rats is negligible. However, a possible involvement of other unknown serine protease(s) that is/are inhibited by camostat mesilate in the pathogenesis of salt-sensitive hypertension in the Dahl salt-sensitive rat cannot be excluded at this point.

In summary, we demonstrated that camostat mesilate and FOY-251 reduced sodium currents in M-1 cells probably by the inhibition of prostasin activity, and that camostat mesilate had both BP lowering and renoprotective effects on Dahl salt-sensitive rats fed with a high-salt diet. Our current findings strongly suggest the possibility that camostat mesilate could represent a new class of anti-hypertensive drugs with renoprotective effects. Because camostat mesilate is orally active and already approved for clinical use for the treatment of reflux esophagitis and chronic pancreatitis in Japan, clinical trials targeting hypertensive patients, especially salt-sensitive hypertensive patients with suppressed renin activity, are definitely required to prove the clinical benefit of camostat mesilate in humans.

Acknowledgement

The authors thank Dr R. Tyler Miller (Case Western Reserve University) for critical reading of the manuscript and helpful discussions.

This work was supported by the following: Grants-in-Aid for Scientific Research from the Ministry of Education, Culture, Sports, Science and Technology in Japan (19590956 to Kenichiro Kitamura, 19590958 to Taku Miyoshi, 18790570 to Naoki Shiraishi, 18790569 to Masataka Adachi, and 18390252 to Kimio Tomita); Salt Science Research Foundation Grant (0728 to Kenichiro Kitamura); Mitsubishi Pharma Research Foundation Grant (to Kenichiro Kitamura); and Suzuken Memorial Foundation Grant (to Kenichiro Kitamura).

References

1 Yu JX, Chao L, Chao J. Prostasin is a novel human serine proteinase from seminal fluid. Purification, tissue distribution, and localization in prostate gland. *J Biol Chem* 1994; **269**:18843–18848.
2 Yu JX, Chao L, Chao J. Molecular cloning, tissue-specific expression, and cellular localization of human prostasin mRNA. *J Biol Chem* 1995; **270**:13483–13489.
3 Adachi M, Kitamura K, Miyoshi T, Narikiyo T, Iwashita K, Shiraishi N, *et al.* Activation of epithelial sodium channels by prostasin in Xenopus oocytes. *J Am Soc Nephrol* 2001; **12**:1114–1121.
4 Vallet V, Chraibi A, Gaeggeler HP, Horisberger JD, Rossier BC. An epithelial serine protease activates the amiloride-sensitive sodium channel. *Nature* 1997; **389**:607–610.
5 Canessa CM, Schild L, Buell G, Thorens B, Gautschi I, Horisberger JD, Rossier BC. Amiloride-sensitive epithelial Na+ channel is made of three homologous subunits. *Nature* 1994; **367**:463–467.
6 Firsov D, Schild L, Gautschi I, Merillat AM, Schneeberger E, Rossier BC. Cell surface expression of the epithelial Na channel and a mutant causing Liddle syndrome: a quantitative approach. *Proc Natl Acad Sci USA* 1996; **93**:15370–15375.
7 Kosari F, Sheng S, Li J, Mak DO, Foskett JK, Kleyman TR. Subunit stoichiometry of the epithelial sodium channel. *J Biol Chem* 1998; **273**:13469–13474.
8 Tong Z, Illek B, Bhagwandin VJ, Verghese GM, Caughey GH. Prostasin, a membrane-anchored serine peptidase, regulates sodium currents in JME/CF15 cells, a cystic fibrosis airway epithelial cell line. *Am J Physiol Lung Cell Mol Physiol* 2004; **287**:L928–L935.
9 Narikiyo T, Kitamura K, Adachi M, Miyoshi T, Iwashita K, Shiraishi N, *et al.* Regulation of prostasin by aldosterone in the kidney. *J Clin Invest* 2002; **109**:401–408.
10 Hughey RP, Mueller GM, Bruns JB, Kinlough CL, Poland PA, Harkleroad KL, *et al.* Maturation of the epithelial Na+ channel involves proteolytic processing of the alpha- and gamma-subunits. *J Biol Chem* 2003; **278**:37073–37082.
11 Bruns JB, Carattino MD, Sheng S, Maarouf AB, Weisz OA, Pilewski JM, *et al.* Epithelial Na+ channels are fully activated by furin- and prostasin-dependent release of an inhibitory peptide from the gamma-subunit. *J Biol Chem* 2007; **282**:6153–6160.
12 Iwashita K, Kitamura K, Narikiyo T, Adachi M, Shiraishi N, Miyoshi T, *et al.* Inhibition of prostasin secretion by serine protease inhibitors in the kidney. *J Am Soc Nephrol* 2003; **14**:11–16.
13 Hirawa N, Uehara Y, Numabe A, Kawabata Y, Gomi T, Ikeda T, *et al.* The implication of renin-angiotensin system on renal injury seen in Dahl salt-sensitive rats. *Am J Hypertens* 1997; **10**:102S–106S.
14 Orosz DE, Hopfer U. Pathophysiological consequences of changes in the coupling ratio of Na,K-ATPase for renal sodium reabsorption and its implications for hypertension. *Hypertension* 1996; **27**:219–227.
15 varez-Guerra M, Garay RP. Renal Na-K-Cl cotransporter NKCC2 in Dahl salt-sensitive rats. *J Hypertens* 2002; **20**:721–727.
16 Aoi W, Niisato N, Miyazaki H, Marunaka Y. Flavonoid-induced reduction of ENaC expression in the kidney of Dahl salt-sensitive hypertensive rat. *Biochem Biophys Res Commun* 2004; **315**:892–896.
17 Otsuka F, Yamauchi T, Kataoka H, Mimura Y, Ogura T, Makino H. Effects of chronic inhibition of ACE and AT1 receptors on glomerular injury in Dahl salt-sensitive rats. *Am J Physiol* 1998; **274**:R1797–R1806.
18 Leenen FH, Yuan B. Prevention of hypertension by irbesartan in Dahl S rats relates to central angiotensin II type 1 receptor blockade. *Hypertension* 2001; **37**:981–984.
19 Tuyen DG, Kitamura K, Adachi M, Miyoshi T, Wakida N, Nagano J, *et al.* Inhibition of prostasin expression by TGF-beta1 in renal epithelial cells. *Kidney Int* 2005; **67**:193–200.
20 Wakida N, Kitamura K, Tuyen DG, Maekawa A, Miyoshi T, Adachi M, *et al.* Inhibition of prostasin-induced ENaC activities by PN-1 and regulation of PN-1 expression by TGF-beta1 and aldosterone. *Kidney Int* 2006; **70**:1432–1438.
21 Netzel-Arnett S, Currie BM, Szabo R, Lin CY, Chen LM, Chai KX, *et al.* Evidence for a matriptase-prostasin proteolytic cascade regulating terminal epidermal differentiation. *J Biol Chem* 2006; **281**:32941–32945.
22 Yamasaki Y, Satomi S, Murai N, Tsuzuki S, Fushiki T. Inhibition of membrane-type serine protease 1/matriptase by natural and synthetic protease inhibitors. *J Nutr Sci Vitaminol* 2003; **49**:27–32.
23 Liu L, Hering-Smith KS, Schiro FR, Hamm LL. Serine protease activity in m-1 cortical collecting duct cells. *Hypertension* 2002; **39**: 860–864.
24 Verghese GM, Gutknecht MF, Caughey GH. Prostasin regulates epithelial monolayer function: cell-specific Gpld1-mediated secretion and functional role for GPI anchor. *Am J Physiol Cell Physiol* 2006; **291**:C1258–C1270.
25 Kim SW, Schou UK, Peters CD, de Seigneux Sophie, Kwon TH, Knepper MA, *et al.* Increased apical targeting of renal epithelial sodium channel subunits and decreased expression of type 2 11beta-hydroxysteroid dehydrogenase in rats with CCl_4-induced decompensated liver cirrhosis. *J Am Soc Nephrol* 2005; **16**:3196–3210.
26 Tetsuo H, Seto S, Yamazaki H, Nagao S, Ozeki S, Yamaguchi T, *et al.* A serine protease inhibitor, nafamostat mesilate, suppresses aldosterone secretions in vivo. *Hypertens Res* 2004; **27**:979–984.
27 Tamaki K, Okuda S, Nakayama M, Yanagida T, Fujishima M. Transforming growth factor-beta 1 in hypertensive renal injury in Dahl salt-sensitive rats. *J Am Soc Nephrol* 1996; **7**:2578–2589.
28 Jones-Burton C, Mishra SI, Fink JC, Brown J, Gossa W, Bakris GL, Weir MR. An in-depth review of the evidence linking dietary salt intake and progression of chronic kidney disease. *Am J Nephrol* 2006; **26**:268–275.
29 He J, Whelton PK. What is the role of dietary sodium and potassium in hypertension and target organ injury? *Am J Med Sci* 1999; **317**:152–159.
30 PROGRESS Collaborative Group. Randomised trial of a perindopril-based blood-pressure-lowering regimen among 6,105 individuals with previous stroke or transient ischaemic attack. *Lancet* 2001; **358**:1033–1041.
31 Matsubara M, Taguma Y, Kurosawa K, Hotta O, Suzuki K, Futaki G. Effect of camostat mesilate on heavy proteinuria in various nephropathies. *Clin Nephrol* 1989; **32**:119–123.
32 Makino H, Onbe T, Kumagai I, Murakami K, Ota Z. A proteinase inhibitor reduces proteinuria in nephrotic syndrome. *Am J Nephrol* 1991; **11**:164–165.
33 Fuller JH, Keen H, Jarrett RJ, Omer T, Meade TW, Chakrabarti R, *et al.* Haemostatic variables associated with diabetes and its complications. *BMJ* 1979; **2**:964–966.
34 Matsubara M, Taguma Y, Kurosawa K, Hotta O, Suzuki K, Ishizaki M. Effect of camostat mesilate for the treatment of advanced diabetic nephropathy. *J Lab Clin Med* 1990; **116**:206–210.

5. ADPKD TRP

東京慈恵会医科大学腎臓・高血圧内科講師　花岡 一成

key words　TRP, Ca^{2+} permeable non-selective cation channel, kidney, ADPKD

動　向

常染色体優性多発性嚢胞腎 autosomal dominant polycystic kidney disease (ADPKD) は，両側の腎臓の皮質および髄質に多数の嚢胞を形成し，腎機能障害が徐々に進行する遺伝性腎疾患である[1]．ADPKDの発症には染色体16p13.3にある*PKD1*遺伝子[2]，あるいは染色体4q21にある*PKD2*遺伝子[3]の異常が関係する．*PKD1*，*PKD2*遺伝子の異常をもつADPKD患者の臨床症状[4]は，腎臓での嚢胞形成をはじめとしてきわめて類似している．近年の研究で*PKD1*，*PKD2*遺伝子産物であるpolycystin1，polycystin2は尿細管細胞で結合してイオンチャンネルとして機能することがわかった[5,6]．本稿ではADPKDの発症に関係のあるpolycystin2のTPRチャンネル機能を中心に，ADPKDの病態を紹介する．なお本稿では，polycystin2をTRPP2として表示する．

A. TRPとは

TRP（transient receptor potential）はイオンチャンネル蛋白の一群で，最初にショウジョウバエ（*Drosophila*）の*trp*とよばれる突然変異体から発見された[7]．正常のショウジョウバエの目に連続的に光を当てると，sustained receptor potentialという持続の長い反応が認められるのに対して，*trp*では細胞外からのCaの流入異常によってtransientな反応がみられることが知られていたが，1989年にCa透過性非選択性陽イオンチャンネルがその原因遺伝子であることがわかった[8]．その後*trp*に相同性の高いTRPCが哺乳類でクローニングされたのをはじめ，現在ではTRPC，TRPV，TRPM，TRPA，TRPP，TRPMLの6つのサブファミリーに分類される50以上の遺伝子がTRPファミリーに属することがわかっている[9,10]．

TRPはKチャンネル同様に6回膜貫通部位を有する膜蛋白で，5～6番の膜貫通部位の間にはチャンネルポアーといわれるイオン透過部位があり，配列の相同性が高く保たれている[11]．TRPは哺乳類以外に，ハエ，線虫，酵母などでも遺伝子が発見され，機能解析により，感覚刺激・圧刺激・温度刺激に反応して，Caその他の陽イオンを透過するCa透過性非選択性陽イオンチャンネルとして働き[12-15]，その異常により各種疾患の原因となることが知られている[16]．各サブファミリーは特徴的な構造を有し，陽イオン選択性に差異がある[17]．

TRPの腎臓における役割としては，Ca再吸収の主要な輸送体（TRPV5，V6）や髄質の浸透圧調節（TRPV4）が知られている[18-22]．さらに，近

年の研究により，足突起の蛋白複合体の構成成分（TRPC6）であることがわかり，その異常により腎炎が発症することが報告されている[23,24]．またADPKD関連では前述のpolycystin2がTRPPサブファミリーに分類され，polycystin1も相同性よりTRPP関連蛋白と認識されている[25,26]．本稿ではADPKDにおけるTPRチャンネルを述べることとする．その他のTPRチャンネルと腎疾患との関連については総説を参照されたい[27]．

B. TRPPサブファミリーとpolycystin1

TRPPサブファミリーには多発性嚢胞腎の責任遺伝子として発見されたPKD2[3]の遺伝子産物polycystin2のほか，PKD2に相同性の高いpolycystin-2L1[28]，polycystin-2L2[29]が属しており，現在はそれぞれTRPP2，TRPP3，TRPP5と呼称されている[25]．TRPP蛋白はほとんどすべての動物種で発見されている．ヒトTRPP2は968個，TRPP3は805個，TRPP5は625個のアミノ酸から構成され，哺乳類間での遺伝子相同性は非常に高く（約90%）保たれている[30]．TRPP2のc末端にはCa結合部位と考えられるEF-hand構造，endoplasmic reritulum（ER）retention sequenceが存在する[31,32]．

PKD1遺伝子産物であるpolycystin1は11回膜貫通部位を有する膜蛋白で，4303個のアミノ酸で構成され[2]，TRPP2とは細胞質内に存在するc末端で蛋白結合している[33,34]．また，polycystin1の第6回目と第7回目の膜貫通部位（T M6-TM7）の間には長い細胞外ループがあり，TRPP2のTM1-TM2と非常に高い相同性をもっている（図1）．

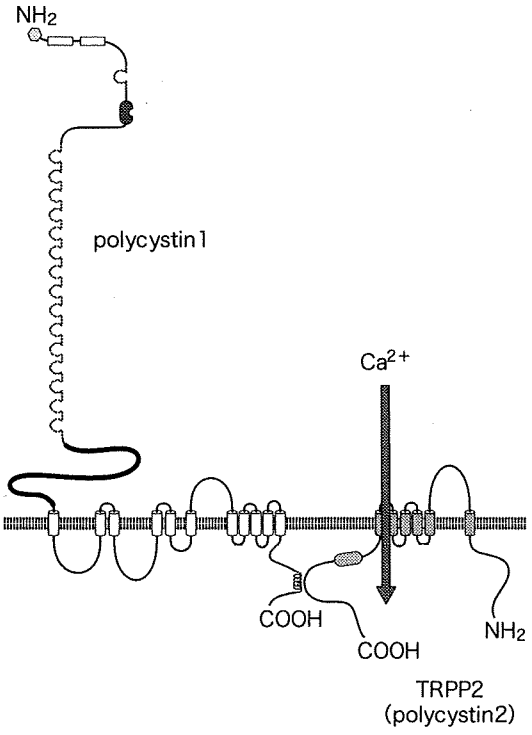

図1　Polycystin1とTRPP2（Polycystin2）

C. TRPP2の局在と機能

1. TRPP2の局在

TRPP2は，尿細管細胞をはじめとする多くの細胞に存在する．細胞内のGolgi装置，ER，細胞膜上全般，尿細管細胞管腔側に存在するprimary ciliaでの発現が報告され，細胞内局在が議論されてきた[35-37]．初期の研究で，正常TRPP2を強制発現させるとERに局在し，各種mutationを発現した場合にTRPP2単独で細胞膜上に移動するmutationがあることがわかり，解析の結果，TRPP2のc末端34個のアミノ酸（Glu787-Ser820）がTRPP2をERにとどめていることが判明した[38]．polycystin1とc末端で結合した正常TRPP2はERにとどまるシグナルを失い，polycystin1-TRPP2蛋白複合体として細胞膜上やprimary ciliaに移動すると考えられた[4]．近年の研究では，TRPP2のc末端部分のリン酸化や蛋白結合がTRPP2の細胞内局在を決定することが解明されつつあり，polycystin1と同様にTRRP2と結合することでTRPP2の細胞膜への移動を促進

する蛋白としてglycogen synthase kinase 3[39], Golgi-and ER-associated protein 14[40] が，一方ER・Golgi装置にとどまるのに必要な蛋白としてPACS-1，PACS-2（phosphofurin-acidic-cluster-sorting protein)[41] が報告されている．その他にも，TRPP2のc末端はIP3受容体[42]，TRPV4[43] と結合し，TRPP2が機能するのに重要な役割を果していると考えられている．

2. TRPP2の細胞膜上での機能

TRPP2はクローニングされた当初からNaチャンネルやTRPなどとの相同性より陽イオンチャンネルとして機能することが予想された[3]．アフリカツメガエルの卵母細胞や動物の継代培養細胞を用いた電気生理の発現実験が試みられたが，細胞膜上でのチャンネル活性を確認することができなかった．著者らはADPKD患者では遺伝子異常が*PKD1*，*PKD2*のいずれの場合でも発現する症状に違いがないことと[1]，polycystin1とTRPP2が同一の尿細管細胞に発現していること[44]，さらにそれぞれのc末端ペプチドを用いた実験で両者が結合して蛋白複合体を形成すると報告[33,34]されていたことをヒントに，両者が結合したheteromultimerが細胞膜上でチャンネル活性をもつとの仮説を立てた．Chinese Hamster由来のCHO細胞にpolycystin1とTRPP2を強制発現させて，蛋白結合，パッチクランプ法によるカルシウムなどの陽イオン電流の確認，蛍光抗体法による細胞内局在の検討を行った結果，この実験系ではpolycystin1とTRPP2が細胞膜上に蛋白複合体を形成し，非選択性陽イオンチャンネル活性を認めることを報告した[4](図2b)．さらにDelmasらは胎児期の腎臓細胞やpolycystin1を強制発現させた神経細胞にegg jelly（REJ）domainに対

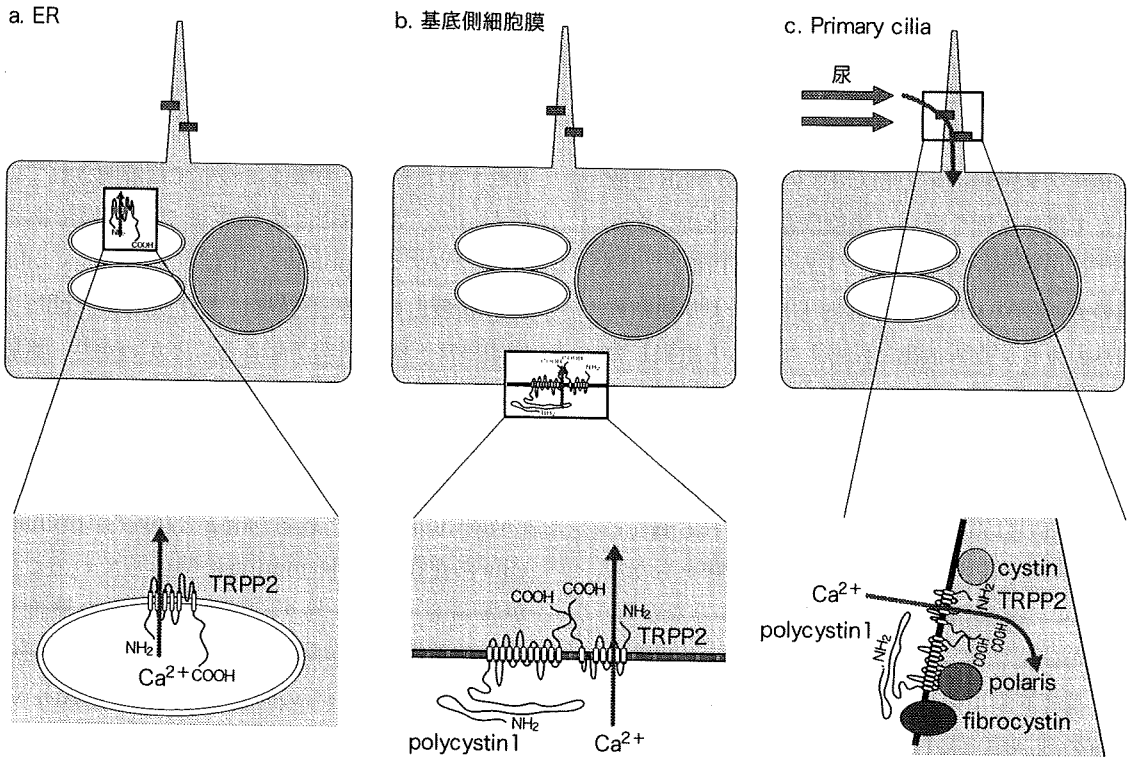

図2　TRPP2の細胞内局在とカルシウムの流入

する特異抗体を投与するとTRPP2のチャンネル活性が増強することを報告し，特定のリガンドがpolycystin1に結合することによりTRPP2チャンネルが制御されていることを示した[45]．

一方，昆虫細胞やヒト胎盤由来細胞を用いた実験ではTRPP2が細胞膜上に単独存在してチャンネル活性をもつと報告されている[46-48]．TRPP2は多くの蛋白と複合体を形成することがわかっていることから，各種細胞に発現している蛋白の種類によりTRPP2を含む蛋白複合体の局在が変化し，細胞膜上でpolycystin1が存在しない条件下でTRPP2のチャンネル活性が観察されたと考えられ，polycystin1が発現していない組織でもTRPP2単独で生理的活性をもつ可能性を示唆している．

3. TRPP2のERでの機能

正常腎臓や，強制発現系において尿細管細胞に発現するTPRP2はERなどの細胞内小器官に多く存在しているため[35-37]，ERでチャンネルとして機能しているかどうかを調べるin vitroの実験が施行されてきた．KoulenらはTPRP2を強制発現させたブタ腎臓由来のLLC-PK1細胞からERを抽出して電気生理を行い，電位依存性のカルシウムイオンの電流を確認したことから，TPRP2はER膜のカルシウムチャンネルとしてERより細胞質内へのカルシウム放出に関与していると主張している[49]（図2a）．ERで観察されたTRPP2が，IP3受容体やrayanodine受容体のようにERの膜上で実際にイオンチャンネルとして機能するのか，あるいは正常では細胞膜に輸送される過程としてERに存在するのみで生理的な意味をもたないのか，まだ結論が出ていない．しかしながら，最近の研究結果から尿細管細胞においてTRPP2は，基底側膜上のほか，後述のごとくにprimary ciliaの細胞膜上に移動し，polycystin1とともにカルシウム流入に関与していると示唆される．

D. Primary ciliaでのTRPP2

1. Primary cilia

Primary ciliaは構造的には細胞膜から連続する表面のcilia膜と，細胞内の基底小体から連続するcentral axonemeとよばれるmicrotubuleで構成されているひも状の構造物で，体内のさまざまな細胞に存在することが知られている[50]．哺乳類のほか，*Drosophila*や*Chlamydomonas elegans*の嗅覚細胞や光受容細胞を用いた研究で，においに関係する化学物質，光刺激，さらに機械的な刺激により，ciliaの細胞膜上に存在するTRPV，TRPNなどのカルシウム透過性チャンネルを介してカルシウムが細胞内に流入することが報告され，現在ではprimary ciliaは細胞外の刺激に反応して細胞内へ情報伝達する器官であると考えられている[51-53]．

2. TRPP2の尿細管細胞primary ciliaでの局在と機能

腎臓の尿細管上皮細胞では，primary ciliaが管腔側細胞膜上に存在していることは以前から知られていたが，その機能については解明されていなかった．ARPKD自然発症モデル動物である*orpk*マウスではpolarisとよばれるprimary ciliaの構成蛋白の遺伝子異常によりprimary ciliaの形態異常・機能異常が起こることがわかり，嚢胞形成にprimary ciliaの機能が関係する可能性が示唆された[54]．さらに，*Chlamydomonas elegans*のsensory neuronにおいてTRPP2とpolycystin1のhomologである*pkd-2*と*lov-1*がprimary ciliaに存在しmale matingに関係していることが報告されるに至り，primary ciliaの機能に*PKD*遺伝子産物が関与することがはじめて証明された[55,56]．これらの研究結果をもとにADPKDの嚢胞形成における TRPP2とpolycystin1の関与が再検討され，正常腎臓の組織を用いた局在の

再検討では，尿細管細胞においてTRPP2とpolycystin1は基底側細胞膜のtight junction付近のほか，primary ciliaの膜上および基底小体に存在していることが確認された[35,46,57,58]．TRPP2-polycystin1蛋白複合体はprimary ciliaにおいては，*PKHD1*遺伝子産物であるfibrocystinのほかcystin，polarisとともにさらに大きな蛋白複合体を形成している[58,59]．一方，ADPKD患者および*PKD1*，*PKD2*遺伝子改変動物の腎組織を観察すると，尿細管細胞では管腔側にprimary ciliaが存在しており，*orpk*マウスで観察されたような形態学的な異常は認められない．

Praetoriusらは，イヌ由来の継代尿細管細胞であるMDCK細胞を培養し，微小な器具を使ってprimary ciliaを固定したのちに，ciliaを引いたり，培養液を還流して圧力をかけたりすると，細胞内へのカルシウムが流入することを報告し，尿流によってprimary ciliaが感知する圧力や機械的な刺激が細胞内に情報として伝達されることを示した[60,61]．Nauliらはフィルター上に培養したpolycystin1，TRPP2共発現細胞の実験系で，管腔側の溶液を還流するとprimary ciliaが機械的刺激として感知し，細胞内へのカルシウム流入が増強することを報告し，Praetorius らによって示された細胞内へのカルシウム流入がTRPP2-polycystin1蛋白複合体を介していることを証明した[62]（図2c）．また，基底側膜に存在するTRPP2-polycystin1蛋白複合体の機能は明らかでない．細胞-細胞接着に関係する情報伝達として細胞内へのカルシウムの流入経路になっていると推測されているが，詳細については今後の検討が必要である．

E. ADPKDの嚢胞形成・拡大

ヒトADPKDの腎臓を用いた研究によれば，嚢胞上皮細胞は細胞の増殖・分化・極性，クロライドイオンなど細胞膜輸送系，細胞のアポプトーシス，細胞外基質の異常などが報告されている[63-65]．collagen matrixの中で培養するとin vitroの嚢胞を形成する特徴があり，嚢胞はcAMP依存性に細胞増殖が起こり，同時にクロライドチャンネルを介して嚢胞液容量が増大し続け，10μm程度の直径であったものが，やがて肉眼で観察できるほどの嚢胞に成長する[66-68]．さらに腎臓の集合管細胞でcAMP依存性に水の再吸収に働くバソプレッシンの作用を抑制するV2受容体阻害剤は，PKD2ノックアウトマウスで嚢胞形成を遅延させることがわかっており，現在世界中でADPKDの患者を対象に第III相の治験が進行している[69]．この他にもADPKDの上皮細胞の増殖についての検討は進み，さまざまな分子標的治療薬が検討されつつある[6]．しかし，polycystin1，TRPP2の異常がどのようにADPKDの細胞機能異常や嚢胞形成をもたらすのか，どうして尿細管の形態を維持することができないのかという疑問に対して現時点までに明確な答えはない．今後のさらなる検討が待たれる．

むすび

ADPKDは，かつて嚢胞の形成を抑えることも，腎障害の進行を抑制することもできず，ただ経過を観察し，両親と同じように病気が進行するのを待っているしかない遺伝性腎疾患と考えられていたが，最近20年で責任遺伝子のクローニング，機能解析，嚢胞拡大機序の研究などが進み，その概念は大きく変りつつある．これらの研究結果をもとに，嚢胞上皮の細胞増殖を抑制するために開発が進んでいる治療薬は，ADPKDの進行を遅らせる素晴らしいツールとなる可能性を秘めているが，嚢胞形成を抑制する根本的な治療とはなりえない．TRPP2-polycystin1蛋白複合体の機能異常とADPKDの嚢胞形成の関係を明らかにすること

は非常に重要で，新たな治療法の開発の指針となると考えられる．今後のさらなる研究の発展を期待し，この項を終えることとする．

文献

1) Gabow PA. Autosomal dominant polycystic kidney disease. N Engl J Med. 1993; 329: 332-42.
2) The European Polycystic Kidney Disease Consortium. The polycystic kidney disease 1 gene encodes a 14 kb transcript and lies within a duplicated region on chromosome 16. Cell. 1994; 77: 881-94.
3) Mochizuki T, Wu G, Hayashi T, et al. PKD2, a gene for polycystic kidney disease that encodes an integral membrane protein. Science. 1996; 272: 1339-42.
4) Wilson PD. Polycystic kidney disease. N Engl J Med. 2004; 350: 151-64.
5) Hanaoka K, Qian F, Boletta A, et al. Co-assembly of polycystin-1 and -2 produces unique cation-permeable currents. Nature. 2000; 408: 990-4.
6) Torres VE, Harris PC, Pirson Y, et al. Autosomal dominant polycystic kidney disease. Lancet. 2007; 369: 1287-301.
7) Montell C, Jones K, Hafen E, et al. Rescue of the Drosophila phototransduction mutation trp by germline transformation. Science. 1985; 230: 1040-43.
8) Montell C, Rubin GM. Molecular characterization of the Drosophila trp locus: a putative integral membrane protein required for phototransduction. Neuron. 1989; 2: 1313-23.
9) Montell C, Birnbaumer L, Flockerzi V, et al. A unified nomenclature for the uperfamily of TRP cation channels. Mol Cell. 2002; 9: 229-31.
10) Ramsey IS, Delling M, Clapham DE. An introduction to TRP channels. Annu Rev Physiol. 2006; 68: 619-47.
11) Lepage PK, Boulay G. Molecular determinants of TRP channel assembly. Biochem Soc Trans. 2007; 35: 81-83.
12) Clapham DE. TRP channels as cellular sensors. Nature. 2003; 426: 517-24.
13) Wang T, Montell C. Phototransduction and retinal degeneration in Drosophila. Pflugers Arch. 2007; 454: 821-47.
14) Christensen AP, Corey DP. TRP channels in mechanosensation: direct or indirect activation ? Nat Rev Neurosci. 2007; 8: 510-21.
15) Kwon Y, Shim HS, Wang X, et al. Control of thermotactic behavior via coupling of a TRP channel to a phospholipase C signaling cascade. Nat Neurosci. 2008; 11: 871-3.
16) Nilius B, Owsianik G, Voets T, et al. Transient receptor potential cation channels in disease. Physiol Rev. 2007; 87: 165-217.
17) Owsianik G, Talavera K, Voets T, et al. Permeation and selectivity of TRP channels. Annu Rev Physiol. 2006; 68: 685-717.
18) Hoenderop JG, van der Kemp AW, Hartog A, et al. Molecular identification of the apical Ca^{2+} channel in 1, 25-dihydroxyvitamin D3-responsive epithelia. J Biol Chem. 1999; 274: 8375-8.
19) Hoenderop JG, van Leeuwen JP, van der Eerden BC, et al. Renal Ca^{2+} wasting, hyperabsorption, and reduced bone thickness in mice lacking TRPV5. J Clin Invest. 2003; 112: 1906-14.
20) Peng JB, Chen XZ, Berger UV, et al. Molecular cloning and characterization of a channel-like transporter mediating intestinal calcium absorption. J Biol Chem. 1999; 274: 22739-46.
21) Bianco SD, Peng JB, Takanaga H, et al. Marked disturbance of calcium homeostasis in mice with targeted disruption of the Trpv6 calcium channel gene. J Bone Miner Res. 2007; 22: 274-85.
22) Mizuno A, Matsumoto N, Imai M, et al. Impaired osmotic sensation in mice lacking TRPV4. Am J Physiol. 2003; 285: C96-101.
23) Reiser J, Polu KR, Moller CC, et al. TRPC6 is a glomerular slit diaphragm-associated channel required for normal renal function. Nat Genet. 2005; 37: 739-44.
24) Mukerji N, Damodaran TV, Winn MP. TRPC6 and FSGS: the latest TRP channelopathy. Biochim Biophys Acta. 2007; 1772: 859-68.
25) Giamarchi A, Padilla F, Coste B, et al. The versatile nature of the calcium-permeable cation TRPP2. EMBO Rep. 2006; 7: 787-93.
26) Qamar S, Vadivelu M, Sandford R. TRP channels and kidney disease: lessons from polycystic kidney disease. Biochem Soc Trans. 2007; 35: 124-8.
27) Hsu YJ, Hoenderop JG, Bindels RJ. TRP channels

in kidney disease. Biochim Biophys Acta. 2007; 1772: 928-36.
28) Nomura H, Turco AE, Pei Y, et al. Identification of PKDL, a novel polycystic kidney disease 2-like gene whose murine homologue is deleted in mice with kidney and retinal defects. J Biol Chem. 1998; 273: 25967-73.
29) Guo L, Schreiber TH, Weremowicz S, et al. Identification and characterization of a novel polycystin family member, polycystin-L2, in mouse and human: sequence, expression, alternative splicing, and chromosomal localization. Genomics. 2000; 15: 64: 241-51.
30) Veldhuisen B, Spruit L, Dauwerse HG, et al. Genes homologous to the autosomal dominant polycystic kidney disease genes (PKD1 and PKD2). Eur J Hum Genet. 1999; 7: 860-72.
31) Cantiello HF. Regulation of calcium signaling by polycystin-2. Am J Physiol. 2004; 286: F1012-29.
32) Qian F, Noben-Truth K. Cellular and molecular function of mucolipins (TRPML) and polycystin2 (TRPP2). Pflugers Arch. 2005; 452: 277-85.
33) Qian F, Germino FJ, Cai Y, et al. PKD1 interacts with PKD2 through a probable coiled-coil domain. Nat Genet. 1997; 16: 179-83.
34) Tsiokas L, Kim E, Arnould T, et al. Homo- and heterodimeric interactions between the gene products of PKD1 and PKD2. Proc Natl Acad Sci USA. 1997; 94: 6965-70.
35) Foggensteiner L, Bevan AP, Thomas R, et al. Cellular and subcellular distribution of polycystin-2, the protein product of the PKD2 gene. J Am Soc Nephrol. 2000; 11: 814-27.
36) Köttgen M, Walz G. Subcellular localization and trafficking of polycystins. Pflugers Arch. 2005; 451: 286-93.
37) Fu X, Wang, Schetle N, et al. The subcellular localization of TRPP2 modulates the function. J Am Soc Nephrol. 2008; 19: 1342-51.
38) Cai Y, Maeda Y, Cedzich A, et al. Identification and characterization of polycystin-2, the PKD2 gene product. J Biol Chem. 1999; 274: 28557-65.
39) Streets AJ, Moon DJ, Kane ME, et al. Identification of an N-terminal glycogen synthase kinase 3 phosphorylation site which regulates the functional localization of polycystin-2 in vivo and in vitro. Hum Mol Genet. 2006; 15: 1465-73.
40) Hidaka S, Konecke V, Osten L, Witzgall R. PIGEA-14, a novel coiled-coil protein affecting the intracellular distribution of polycystin-2. J Biol Chem. 2004; 279: 35009 -16.
41) Köttgen M, Benzing T, Simmen T, et al. Trafficking of TRPP2 by PACS proteins represents a novel mechanism of ion channel regulation. EMBO J. 2005 23; 24: 705-16.
42) Li Y, Wright JM, Qian F, et al. Polycystin 2 interacts with type I inositol 1, 4, 5-trisphosphate receptor to modulate intracellular Ca^{2+} signaling. J Biol Chem. 2005; 280: 41298-306.
43) Köttgen M, Buchholz B, Garcia-Gonzalez MA, et al. TRPP2 and TRPV4 form a polymodal sensory channel complex. J Cell Biol. 2008; 182: 437-47.
44) Ong AC, Ward CJ, Butler RJ, et al. Coordinate expression of the autosomal dominant polycystic kidney disease proteins, polycystin-2 and polycystin-1, in normal and cystic tissue. Am J Pathol. 1999; 154: 1721-9.
45) Delmas P, Nauli SM, Li X, et al. Gating of the polycystin ion channel signaling complex in neurons and kidney cells. FASEB J. 2004; 18: 740-2.
46) González-Perrett S, Kim K, Ibarra C, et al. Polycystin-2, the protein mutated in autosomal dominant polycystic kidney disease (ADPKD), is a Ca^{2+}-permeable nonselective cation channel. Proc Natl Acad Sci USA. 2001; 98: 1182-7.
47) Li Q, Montalbetti N, Shen PY, et al. Alpha-actinin associates with polycystin-2 and regulates its channel activity. Hum Mol Genet. 2005; 14: 1587-603.
48) Montalbetti N, Li Q, Wu Y, et al. Polycystin-2 cation channel function in the human syncytiotrophoblast is regulated by microtubular structures. J Physiol. 2007; 579: 717-28.
49) Koulen P, Cai Y, Geng L, et al. Polycystin-2 is an intracellular calcium release channel. Nat Cell Biol. 2002; 4: 191-7.
50) Ibanez-Tallon I, Heintz N, Omran H. To beat or not to beat: roles of cilia in development and disease. Hum Mol Genet. 2003; 12: R27-35.
51) Bae YK, Barr MM. Sensory roles of neuronal cilia: cilia development, morphogenesis, and function in C. elegans. Front Biosci. 2008; 13: 5959-74.

52) Satir P, Christensen ST. Overview of structure and function of mammalian cilia. Annu Rev Physiol. 2007; 69: 377-400.
53) Zariwala MA, Knowles MR, Omran H. Genetic defects in ciliary structure and function. Annu Rev Physiol. 2007; 69: 423-50.
54) Pazour GJ, Dickert BL, Vucica Y, et al. Chlamydomonas IFT88 and its mouse homologue, polycystic kidney disease gene tg737, are required for assembly of cilia and flagella. J Cell Biol. 2000; 151: 709-18.
55) Barr MM, DeModerna J, Braun D, et al. The Caenorhabditis elegans autosomal dominant polycystic kidney disease gene homologs lov-1 and pkd-2 act in the same pathway. Curr Biol. 2001; 11: 1341-6.
56) Barr MM, Sternberg PW. A polycystic kidney-disease gene homologue required for male mate behavior in C. elegans. Nature. 1999; 401: 386-9.
57) Obermüller N, Gallagher AR, Cai Y, et al. The rat pkd2 protein assumes distinct subcellular distributions in different organs. Am J Physiol. 1999; 277: F914-25.
58) Yoder BK, Hou X, Guay-Woodford LM. The polycystic kidney disease proteins, polycystin-1, polycystin-2, polaris, and cystin, are co-localized in renal cilia. J Am Soc Nephrol. 2002; 13: 2508-16.
59) Ward CJ, Yuan D, Masyuk TV, et al. Cellular and subcellular localization of the ARPKD protein; fibrocystin is expressed on primary cilia. Hum Mol Genet. 2003; 12: 2703-10.
60) Praetorius HA, Spring KR. Bending the MDCK cell primary cilium increases intracellular calcium. J Membr Biol. 2001; 184: 71-9.
61) Praetorius HA, Spring KR. A physiological view of the primary cilium. Annu Rev Physiol. 2005; 67: 515-29.
62) Nauli SM, Alenghat FJ, Luo Y, et al. Polycystins 1 and 2 mediate mechanosensation in the primary cilium of kidney cells. Nat Genet. 2003; 33: 129-37.
63) Sullivan LP, Wallace DP, Grantham JJ. Epithelial transport in polycystic kidney disease. Physiol Rev. 1998; 78: 1165-91.
64) Igarashi P, Somlo S. Genetics and pathogenesis of polycystic kidney disease. J Am Soc Nephrol. 2002; 13: 2384-98.
65) Wilson PD. Polycystic kidney disease. N Engl J Med. 2004; 350: 151-64.
66) Hanaoka K, Devuyst O, Schwiebert EM, et al. A role for CFTR in human autosomal dominant polycystic kidney disease. Am J Physiol. 1996; 270: C389- 99.
67) Hanaoka, K, Guggino WB. cAMP regulates cell proliferation and cyst formation in autosomal polycystic kidney disease cell. J Am Soc Nephrol. 2000; 11: 1179- 87.
68) Yamaguchi T, Wallace DP, Magenheimer BS, et al. Calcium restriction allows cAMP activation of the B-Raf/ERK pathway, switching cells to a cAMP-dependent growth-stimulated phenotype. J Biol Chem. 2004; 279: 40419-30.
69) Bennett WM. V2 receptor antagonists in cystic kidney diseases: An exciting step towards a practical treatment. J Am Soc Nephrol. 2005; 16: 838-9.

Pflugers Arch - Eur J Physiol (2009) 457:845–856
DOI 10.1007/s00424-008-0561-y

PKD1 haploinsufficiency is associated with altered vascular reactivity and abnormal calcium signaling in the mouse aorta

Nicole Morel · Greet Vandenberg · Ali K. Ahrabi · Nathalie Caron · Fanny Desjardins · Jean-Luc Balligand · Shigeo Horie · Olivier Devuyst

Received: 7 May 2008 / Revised: 11 July 2008 / Accepted: 15 July 2008 / Published online: 5 August 2008

Abstract Mutations in *PKD1* are associated with autosomal dominant polycystic kidney disease (ADPKD), which leads to major cardiovascular complications. We used mice with a heterozygous deletion of *Pkd1* ($Pkd1^{+/-}$) and wild-type ($Pkd1^{+/+}$) littermates to test whether *Pkd1* haploinsufficiency is associated with a vascular phenotype in different age groups. Systolic blood pressure measured by the tail-cuff method was similar up to 20 weeks of age, but significantly higher in 30-week-old $Pkd1^{+/-}$ compared to $Pkd1^{+/+}$. By contrast, similar telemetric recordings were obtained in unrestrained $Pkd1^{+/-}$ and $Pkd1^{+/+}$ mice. The contractile responses evoked by KCl or phenylephrine were similar in young animals but increased in abdominal aortas of 30-week-old $Pkd1^{+/-}$ mice, and acetylcholine-evoked relaxation was depressed. Basal cytosolic calcium, KCl, and phenylephrine-evoked calcium signals were significantly lower in the $Pkd1^{+/-}$ aortas, whereas calcium release evoked by caffeine or thapsigargin was significantly larger. These changes were paralleled with a significant change in the mRNA expression of *Pkd2*, *Trpc1*, *Orai1*, and *Serca2a* in the aortas from $Pkd1^{+/-}$ vs. $Pkd1^{+/+}$. These results are the first to indicate that haploinsufficiency in *Pkd1* is associated with altered intracellular calcium homeostasis and increased vascular reactivity in the aorta with compensatory changes in transport proteins involved in the calcium signaling network.

Keywords Polycystin-1 · Polycyctin-2 · ADPKD · Aorta · Contraction · Calcium signaling

N. Morel (✉) · G. Vandenberg
Laboratoire de Physiologie Cellulaire,
Université Catholique de Louvain,
Avenue Hippocrate 55,
UCL 5540 Brussels, Belgium
e-mail: nicole.morel@uclouvain.be

A. K. Ahrabi · O. Devuyst
Unité de Néphrologie, Université Catholique de Louvain,
Avenue Hippocrate 54,
UCL 5450 Brussels, Belgium

F. Desjardins · J.-L. Balligand
Unité de Pharmacothérapie, Université Catholique de Louvain,
Avenue Emmanuel Mounier, 52,
UCL 5349 Brussels, Belgium

S. Horie
Department of Urology, School of Medicine, Teikyo University,
2-11-1 Kaga,
Tokyo 173-8605, Japan

N. Caron
Laboratoire de Physiologie,
Facultés Universitaires Notre-Dame de la Paix,
Rue de Bruxelles, 61,
5000 Namur, Belgium

Introduction

Autosomal dominant polycystic kidney disease (ADPKD) is the most frequently inherited nephropathy and an important cause of end-stage renal disease. Mutations in two genes, *PKD1* and *PKD2*, have been associated with ADPKD. Mutations in *PKD1* account for approximately 85% of the affected families, and they are associated with a renal disease that progresses more rapidly than in *PKD2* families [30]. *PKD1* and *PKD2* encode integral membrane proteins, polycystin-1 (PC1) and polycystin-2 (PC2), which are located in the primary cilium and interact in vivo to

regulate various signaling pathways involved in the proliferation and differentiation of renal tubular cells [37]. Since PC2 shares significant sequence homology with voltage-dependent Ca^{2+} channels and transient receptor potential channels (TRP) and forms a nonselective cation channel highly permeable to Ca^{2+}, it has been suggested that the association of PC1 with PC2 constitutes a functional complex that is involved in regulating intracellular Ca^{2+} homeostasis [10, 24].

Cardiovascular complications are the main cause of death in patients with ADPKD. Hypertension is frequently an inaugural manifestation of ADPKD, present in approximately 50% of ADPKD patients with normal renal function [38]. Its development is accompanied by a reduction in renal blood flow, a more rapid progression of renal disease, and a high incidence of left ventricular hypertrophy [30, 38]. An impaired endothelium-dependent relaxation may contribute to vasoconstriction, and thereby, to the progressive loss of renal function in the disease [28, 42]. Both PC1 and PC2 are expressed in the endothelium and vascular smooth muscle cells (VSMC) lining large arteries in man and mouse [9, 15]. Mouse embryos homozygous for *Pkd1* or *Pkd2* null mutations show hydrops fetalis, localized hemorrhages, and increased microvascular permeability [3, 15, 23, 43]. Furthermore, heterozygous *Pkd2*$^{+/-}$ arteries develop increased contractility [32], have altered VSMC intracellular Ca^{2+} homeostasis, and increased cAMP levels [16, 33]. Taken together, these studies suggest that a loss of function or altered dosage of PC1–PC2 in the vasculature could play a part in the early development of hypertension in ADPKD. However, it is unknown whether haploinsufficiency in *PKD1*—the most frequent situation in ADPKD patients—is associated with alterations in Ca^{2+} signaling or changes in vascular tone and reactivity which could lead to impaired blood pressure control.

In the present study, we used a well-established *Pkd1* mouse model [23] to test whether *Pkd1* haploinsufficiency is associated with vascular dysfunction, in relation with intracellular Ca^{2+} homeostasis. Like other *Pkd1* null mutants, the homozygous *Pkd1*$^{-/-}$ mice die in utero with massive cystic kidneys, hydrops fetalis, and cardiovascular defects [23]. By contrast, there is no consistent phenotype in heterozygous *Pkd1*$^{+/-}$ mice which do not develop renal cysts and renal failure until a very old age [21, 23]. Our investigations reveal for the first time that reduced *PKD1* dosage is associated with an age-dependent increase in vascular reactivity, with altered intracellular Ca^{2+} homeostasis in the aorta and compensatory changes in transport proteins involved in the Ca^{2+} signaling network. These data give insights into the biology of PC1 and vascular damage in ADPKD.

Materials and methods

Pkd1 mice and sampling

Experiments were conducted on three groups of age-matched, male mice (aged 12, 20, and 30 weeks, respectively) with a targeted deletion of exons 2–5 and part of exon 6 of *Pkd1*, resulting in a null allele [23]. The experiments were conducted in accordance with the National Research Council Guide for the Care and Use of Laboratory Animals and were approved by the local Ethics Committee.

Blood pressure and continuous telemetry recording

Systolic blood pressure (SBP) was measured by the tail-cuff method in conscious, restrained animals (Physiograph Narco, Houston, TX, USA), on two different days. Four to six successive measurements were averaged. Continuous recording of blood pressure signals (and heart rate, derived from pressure waves) from the aortic arch was performed in conscious, unrestrained animals with surgically implanted, miniaturized telemetry devices (Datascience, USA). Briefly, under anesthesia with a mixture of ketamine and xylazine, the left common carotid artery was isolated and the tip of the catheter was retrogradely inserted into the artery until the aortic arch. The catheter was connected to the body of the implant, placed in a subcutaneous pouch in the right flank. After 1 week of recovery, long-term (24 h) online recordings were digitized (range, 20 to 2,000 Hz) and stored for further analysis [12, 27].

Measurement of aorta morphology and contractile tension

A 2-mm segment of abdominal aorta was mounted in a myograph containing physiological solution (composition in mmol/L: NaCl 122, KCl 5.9, $NaHCO_3$ 15, glucose 10, $MgCl_2$ 1.25, and $CaCl_2$ 1.25, gassed with a mixture of 95% O_2–5% CO_2). Passive tension–diameter relationship was established to estimate diameter at 100 mmHg (L100) and vessel diameter was set at 0.9×L100. After 30 min recuperation time, the aorta was contracted by changing the physiological solution in the bath to a high-KCl, depolarizing solution (composition in mmol/L: NaCl 27, KCl 100, $NaHCO_3$ 15, glucose 10, $MgCl_2$ 1.25, $CaCl_2$ 1.25). Acetylcholine (1 μmol/L) was used to verify the integrity of the endothelium. Contraction to phenylephrine was measured by cumulatively increasing the concentration of phenylephrine in the bath solution. When required, arteries were incubated with *N*-nitro-L-arginine (NNA, 0.1 mmol/L) for 30 min before stimulation. For the relaxation studies, the arteries were contracted with phenylephrine (1 μmol/L). At the end of the experiment, myo-

graph was put on the stage of an inverted microscope to measure wall thickness. Contraction was normalized for the length of the aortic segment and expressed as millinewton per millimeter.

Measurement of aorta contractile tension and cytosolic calcium concentration

Aortic rings isolated from 18- to 22-week-old mice were endothelium-denuded by gentle rubbing and were incubated for 3 h at room temperature in physiological solution containing 5 μmol/L fura-PE3 acetoxymethyl ester and 0.05% Cremophor EL. The rings were mounted between two hooks under a tension of 8 mN in a 3-ml cuvette filled with physiological solution (composition as above) at 37°C gassed with a 95–5% mixture of O_2 and CO_2. All solutions contained NNA (0.1 mmol/L). The cuvette was part of a fluorimeter (CAF, JASCO, Tokyo) that allowed simultaneous estimation of the calcium signal while the muscle tone was measured by an isometric force transducer. The Ca^{2+} signal was measured as previously reported [8]. To measure Ca^{2+} release from the sarcoplasmic reticulum (SR), aorta was perfused for 2.5 min with Ca^{2+}-free solution (same composition as the physiological solution without $CaCl_2$ and with 0.1 mmol/L ethylene glycol bis(2-aminoethyl ether)-*N*,*N*,*N*′,*N*′-tetraacetic acid [EGTA]) before Ca^{2+} release was evoked by phenylephrine (1 μmol/L), caffeine (10 mmol/L), or thapsigargin (1 μmol/L) added in the Ca^{2+}-free solution. At the end of the experiment, the fura-2-Ca^{2+} signal was calibrated and cytosolic calcium concentration was calculated as described previously [7]. Ca^{2+} release was estimated from the area under the curve, corrected for the baseline value estimated by interpolation of the data points recorded during 1 min before the application of the stimulation and after completion of the release phase.

Aorta permeabilization

Aortas were permeabilized by using the Ca^{2+} ionophore ionomycin (10 μmol/L—2 min), which allowed to equilibrate the intracellular and extracellular Ca^{2+} concentration. Aortas were thereafter incubated in Ca^{2+}-free solution containing 1 mmol/L EGTA. Contraction was evoked by adding Ca^{2+} in the solution. The added Ca^{2+} was calculated in order to obtain the desired pCa (−log Ca^{2+} concentration). Mg^{2+} was adjusted to 1.25 mmol/L [25].

Real-time q-PCR

Total RNA from 20-week-old mouse aorta and kidney was extracted with Trizol (Invitrogen, Merelbeke, Belgium), treated with DNase I, and reverse-transcribed into cDNA with SuperScript III Rnase H Reverse Transcriptase (Invitrogen). The quality and quantity of RNA were evaluated using the 2100 BioAnalyzer (Agilent Technologies, Palo Alto, CA, USA). The primers (Table 1) were designed using Beacon Designer 2.0 (Premier Biosoft International, Palo Alto, CA, USA). The PCR products were sequenced by Genome Express. The efficiency of each set of primers was determined by dilution curves and the Ct differences between the reference (*Gapdh*) and target genes calculated for each sample of each genotype. The formula used to quantify the relative changes in target over *Gapdh* mRNAs between the two groups is derived from the $2^{-\Delta\Delta Ct}$ formula as described by Pfaffl [29]. The threshold Ct values were obtained from nine different mice in each group for aorta and four mice for kidney. Analysis of housekeeping gene expression stability between genotypes was done using the geNorm software [40].

Drugs

Fura-PE3 acetoxymethyl ester was from Calbiochem (Euro-Biochem, Bierges, Belgium). All other compounds were from Sigma (Sigma-Aldrich, Bornem, Belgium).

Statistical analysis

Data are presented as the means±SEM. $LogEC_{50}$ (pD_2) values were calculated by nonlinear curve fitting of the individual concentration–effect curves (GraphPad Prism) and were used for the statistical analysis. Comparisons were made by Student's *t* test or ANOVA. Concentration–effect curves were compared by two-way ANOVA (GraphPad Prism). *P* values <0.05 were considered significant.

Results

Biometric parameters and blood pressure control in *Pkd1* mice

The biometric parameters of the three age groups of *Pkd1* mice are given in Table 2. The $Pkd1^{+/+}$ and $Pkd1^{+/-}$ mice had a similar body weight in each age group. Tail-cuff plethysmography revealed similar SBP in both groups up to 20 weeks, while SBP of $Pkd1^{+/-}$ was significantly higher than that of $Pkd1^{+/+}$ at age 30 weeks. However, no difference in diastolic and systolic blood pressure was observed between $Pkd1^{+/-}$ and $Pkd1^{+/+}$ aged 20 to 30 weeks when using a telemetry system in unrestrained animals. No significant cardiac or aortic wall hypertrophy and no difference in aortic internal diameter at a transmural pressure of 100 mmHg were observed between $Pkd1^{+/-}$ and $Pkd1^{+/+}$.

Table 1 Sequences of primers and efficiency of q-PCR reactions

Gene	Sequence of primers	Amplicons (bp)	Efficiency
Gapdh	Sense TGCACCACCAACTGCTTAGC Antisense GGATGCAGGGATGATGTTCT	176	1.04±0.03
18s Rna	Sense GTAACCCGTTGAACCCCATT Antisense CCATCCAATCGGTAGTAGCG	151	0.98±0.02
beta-Actin	Sense TGCCCATCTATGAGGGCTAC Antisense CCCGTTCAGTCAGGATCTTC	102	1.03±0.04
Hprt1	Sense ACATTGTGGCCCTCTGTGTG Antisense TTATGTCCCCCGTTGACTGA	162	0.99±0.01
Cyclophilin a	Sense CGTCTCCTTCGAGCTGTTTG Antisense CCACCCTGGCACATGAATC	139	1.02±0.02
36b4	Sense CTTCATTGTGGGAGCAGACA Antisense TTCTCCAGAGCTGGGTTGTT	150	1.02±0.02
Nos3	Sense CTCCCAGCTGTGTCCAACAT Antisense CACACAGCCACATCCTCAAG	149	1.04±0.04
Pkd1	Sense TAGGGCTCCTGGTGAACCTT Antisense CCAGACCACAGTTGCACTCA	150	1.02±0.06
Pkd2	Sense GGAGGAACTTCTGGCTGGA Antisense ACAGGCTGAAACTGCCAAGA	151	0.93±0.06
Trpc1	Sense AGAGCTGCAGTCCTTCGTTG Antisense GCTCGAGCAAACTTCCATTC	150	0.98±0.03
Stim1	Sense AGCTGGAATCACACAGCTCA Antisense TATTTTCTCAGCCCCCTCCT	149	0.98±0.03
Orai1	Sense CAGACCATGACTACCCACCA Antisense ACCGAGTTGAGGTTGTGGAC	148	0.96±0.04
Chop10	Sense CCCAGGAAACGAAGAGGAAG Antisense CCTCCTGGGCCATAGAACT	155	1.06±0.02
Edn1	Sense CTGGGAGGTTCTTCCAGGT Antisense TTTGGGCCCTGAGTTCTTTT	148	1.04±0.06
Serca2b	Sense GGTGGTCTGGGTCTACAGC Antisense AACCTCCTTCACCAGCCAAT	171	1.05±0.02
Serca2a	Sense GAACCTTTGCCGCTCATTTT Antisense TCCAGTATTGCGGGTTGTTC	146	0.99±0.06
Ren1	Sense ATCTTTGACACGGGTTCAGC Antisense TGATCCGTAGTGGATGGTGA	150	1.02±0.04

Age-dependent endothelial dysfunction and increased contractile responses in $Pkd1^{+/-}$ aortas

The endothelium-dependent relaxation evoked by acetylcholine was similar in $Pkd1^{+/-}$ and $Pkd1^{+/+}$ mice up to 20 weeks of age but it was significantly attenuated in 30-week-old $Pkd1^{+/-}$ aortas (Fig. 1a). Similarly, no difference was observed in the contractile responses to phenylephrine in aortic segments from 12- and 20-week-old *Pkd1* mice, whereas, at age 30 weeks, the contractions were significantly larger in $Pkd1^{+/-}$ aortas despite unchanged sensitivity to phenylephrine (Fig. 1b, Table 3). The NOS inhibitor NNA shifted the phenylephrine concentration–effect curves to the left but did not affect the difference between $Pkd1^{+/+}$ and $Pkd1^{+/-}$ (Fig. 1b).

The contractile response to KCl was not different between 12-week-old samples, but at 20 and 30 weeks, aortas from $Pkd1^{+/-}$ developed significantly larger contractions than $Pkd1^{+/+}$ aortas (2.2±0.2 and 2.9±0.2 mN/mm at 20 weeks, n=17, P<0.05, 1.7±0.2 and 2.5±0.3 mN/mm at 30 weeks, n=12, P<0.05 in $Pkd1^{+/+}$ and $Pkd1^{+/-}$, respectively).

Alteration of Ca^{2+} handling in vascular smooth muscle from $Pkd1^{+/-}$ aortas

In endothelium-denuded aorta, basal cytosolic Ca^{2+} was lower in $Pkd1^{+/-}$ compared to $Pkd1^{+/+}$ (104±9 vs. 146± 3 nmol/L, n=19 pairs, P<0.05) (Fig. 2a). KCl-depolarization simultaneously increased global cytosolic Ca^{2+} and contractile tension (Fig. 2b): the increase in calcium was significantly smaller in $Pkd1^{+/-}$ samples, while simultaneous contraction was enhanced. Accordingly, a significantly higher ratio of contraction to cytosolic Ca^{2+} concentration was observed in $Pkd1^{+/-}$ vs. $Pkd1^{+/+}$ aortas

Table 2 Biometric and hemodynamic parameters of *Pkd1* mice

	$Pkd1^{+/+}$	$Pkd1^{+/-}$
Weight (g)		
12 weeks	25.5±0.6 (8)	24.5±0.5 (7)
20 weeks	27.7±0.6 (18)	27.4±0.8 (18)
30 weeks	27.7±0.7 (8)	29.4±0.7 (7)
Systolic blood pressure, tail-cuff (mmHg)		
12 weeks	117±5 (6)	122±6 (6)
20 weeks	117±10 (5)	114±6 (5)
30 weeks	101±6 (6)	141±6 (6) *
Systolic blood pressure, radiotelemetry (mmHg)		
20 weeks	114±2.2 (4)	118±1.6 (4)
30 weeks	121±2.4 (4)	115±1.9 (4)
Diastolic blood pressure, radiotelemetry (mmHg)		
20 weeks	88.8±1.8 (4)	90.7±1.5 (4)
30 weeks	97.6±2.3 (4)	91.4±1.4 (4)
Heart/body weight (mg/g)		
12 weeks	5.42±0.30 (5)	5.84±0.29 (5)
20 weeks	4.16±0.08 (4)	3.86±0.10 (4)
30 weeks	3.95±0.17 (5)	4.00±0.04 (5)
Aorta wall thickness (μ)		
12 weeks	39.9±3.8 (4)	35.8±2.4 (4)
20 weeks	54.1±1.0 (4)	55.9±2.0 (4)
30 weeks	55.3±2.3 (7)	53.7±2.3 (7)
Aorta internal diameter (μ)		
12 weeks	1,059±13 (6)	1,038±20 (6)
20 weeks	1,166±40 (12)	1,076±23 (9)
30 weeks	1,185±39 (9)	1,018±29 (7)

Data are the means±SEM from (*n*) animals
*$P<0.05$ vs. $Pkd1^{+/+}$

(6.9±1.1 and 4.8±0.6 mN per 100 nmol/L increase in cytosolic Ca^{2+}, respectively, $n=18$, $P<0.05$).

The α1-adrenergic agonist phenylephrine is known to increase cytosolic Ca^{2+} both by the release of intracellular Ca^{2+} and the activation of Ca^{2+} entry through plasmalemmal channels. In the absence of stimulation, removal of Ca^{2+} from the perfusion solution produced a decrease in cytosolic Ca^{2+} that was reversed after the readdition of Ca^{2+} into the perfusion solution (not shown). Phenylephrine (1 μmol/L) applied during perfusion of the artery with Ca^{2+}-free solution produced a transient increase in Ca^{2+} signal and contraction (Fig. 2c). The intracellular Ca^{2+} release was significantly smaller in $Pkd1^{+/-}$ aortas, contrasting with a similar contraction. In the presence of phenylephrine, readdition of Ca^{2+} into the perfusion solution produced a rapid increase in contractile tension and in cytosolic Ca^{2+}, which stabilized at a level higher than the basal resting level (Fig. 2c). Although the increase in cytosolic Ca^{2+} was similar in $Pkd1^{+/-}$ and $Pkd1^{+/+}$, the amplitude of the simultaneous contraction was twice larger in $Pkd1^{+/-}$ aortas compared to WT ($P<0.05$).

To further investigate the Ca^{2+} storage capacity of the sarcoplasmic reticulum (SR), Ca^{2+} release was evoked by caffeine or the SERCA inhibitor thapsigargin in arteries bathed in Ca^{2+}-free solution (Fig. 3). Caffeine (10 mmol/L) or thapsigargin (1 μmol/L) did not evoke a significant change in cytosolic Ca^{2+} in $Pkd1^{+/+}$ mice, but produced a transient increase in cytosolic Ca^{2+} in $Pkd1^{+/-}$ aorta. The addition of Ca^{2+} into the bathing solution after store depletion with caffeine evoked a rapid increase in Ca^{2+} signal, which was significantly smaller in $Pkd1^{+/-}$ compared to $Pkd1^{+/+}$ (Fig. 3a, b), while Ca^{2+} entry after store depletion with thapsigargin produced a similar increase in cytosolic Ca^{2+} in $Pkd1^{+/-}$ and $Pkd1^{+/+}$ (Fig. 3c, d).

Permeabilized $Pkd1^{+/-}$ aorta develops increased contractile tension

In aorta permeabilized with the Ca^{2+} ionophore ionomycin, increasing the free Ca^{2+} concentration in the bath solution evoked a concentration-dependent contraction (Fig. 4). The contractile response as a function of the pCa was larger in $Pkd1^{+/-}$ aorta vs. $Pkd1^{+/+}$. However, the pCa producing half-maximum response was unchanged (6.87±0.18 vs. 7.03±0.17, respectively), suggesting that the sensitivity of the contraction to Ca^{2+} was not different.

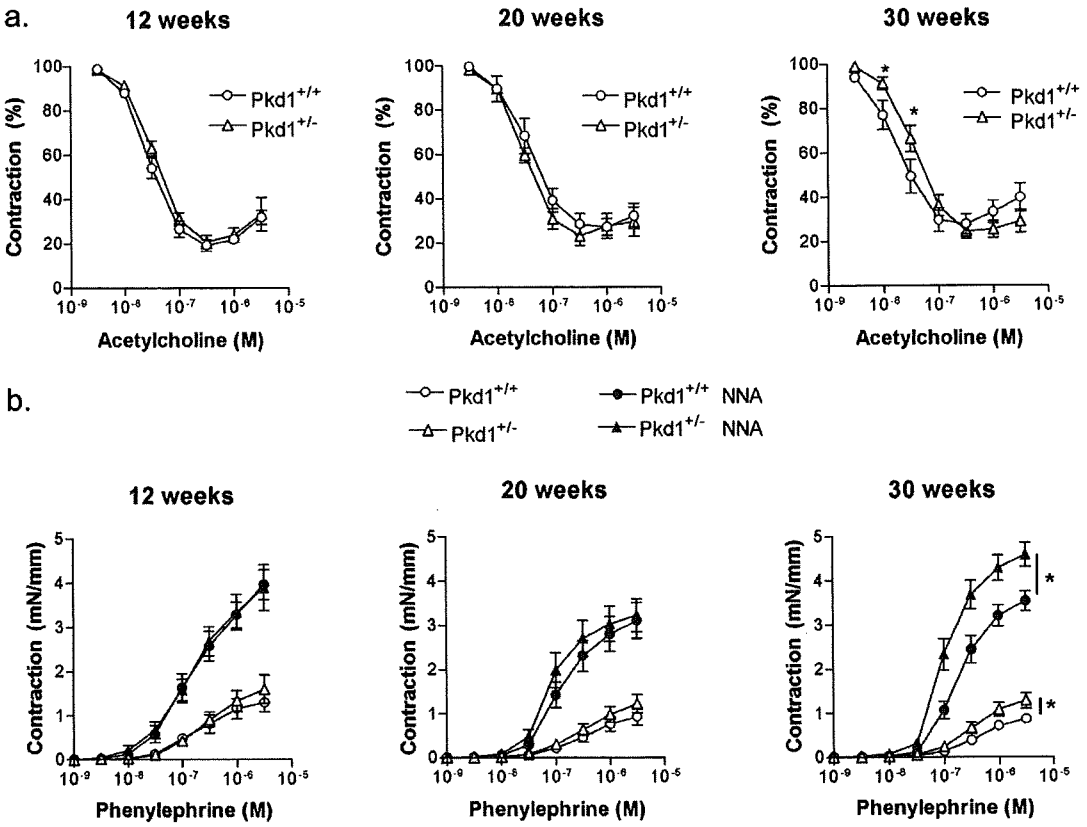

Fig. 1 Concentration–effect curves of acetylcholine-evoked relaxation and phenylephrine-evoked contraction in aortas isolated from 12-, 20-, and 30-week-old $Pkd1^{+/+}$ and $Pkd1^{+/-}$. **a** Aortas were precontracted with phenylephrine (1 μmol/L). Acetylcholine was added into the physiological solution when contraction was stable. Data expressed as percent of the contraction evoked by phenylephrine before the addition of acetylcholine are the means±SEM from eight determinations. *P<0.05, significant difference in the effect of acetylcholine between $Pkd1^{+/-}$ and $Pkd1^{+/+}$ (Student's t test). **b** Contraction was evoked by cumulative increase in phenylephrine concentration in the bathing solution. After washing, aortas were incubated with NNA (100 μmol/L) for 30 min before the concentration–response curve to phenylephrine was resumed. Data are expressed as the means±SEM from six to eight determinations. *P<0.05, between curves obtained in $Pkd1^{+/-}$ and in $Pkd1^{+/+}$ (ANOVA)

Differential transcriptional regulation in $Pkd1^{+/-}$ aortas and kidneys

Real-time q-PCR was used to test the differential expression of transcripts primarily involved in endothelial reactivity (*eNOS*, *endothelin*) and intracellular Ca^{2+} regulation (*Serca2a* and *2b*, *Pkd2*, *Trpc1*, *Stim1*, and *Orai1*) (Fig. 5). As expected, the expression levels of *Pkd1* mRNA in $Pkd1^{+/-}$ was approximately 50% of the wild-type level. The levels of *Pkd2* and *Trpc1* mRNA were significantly

Table 3 Phenylephrine pD_2 values ($-\log ED_{50}$) with(out) NNA

	Without NNA		With NNA	
	$Pkd1^{+/+}$	$Pkd1^{+/-}$	$Pkd1^{+/+}$	$Pkd1^{+/-}$
12 weeks (n=6)	6.60±0.09	6.55±0.09	6.73±0.16*	6.82±0.10*
20 weeks (n=8)	6.40±0.09	6.37±0.07	6.86±0.06*	7.01±0.10*
30 weeks (n=8)	6.40±0.06	6.46±0.05	6.71±0.07*	6.97±0.08*, **

pD_2 values were calculated by nonlinear curve fitting of the individual concentration–effect curves. Data are the means±SEM from n determinations

*P<0.05 vs. without NNA; **P<0.05 vs. $Pkd1^{+/+}$ at the same age

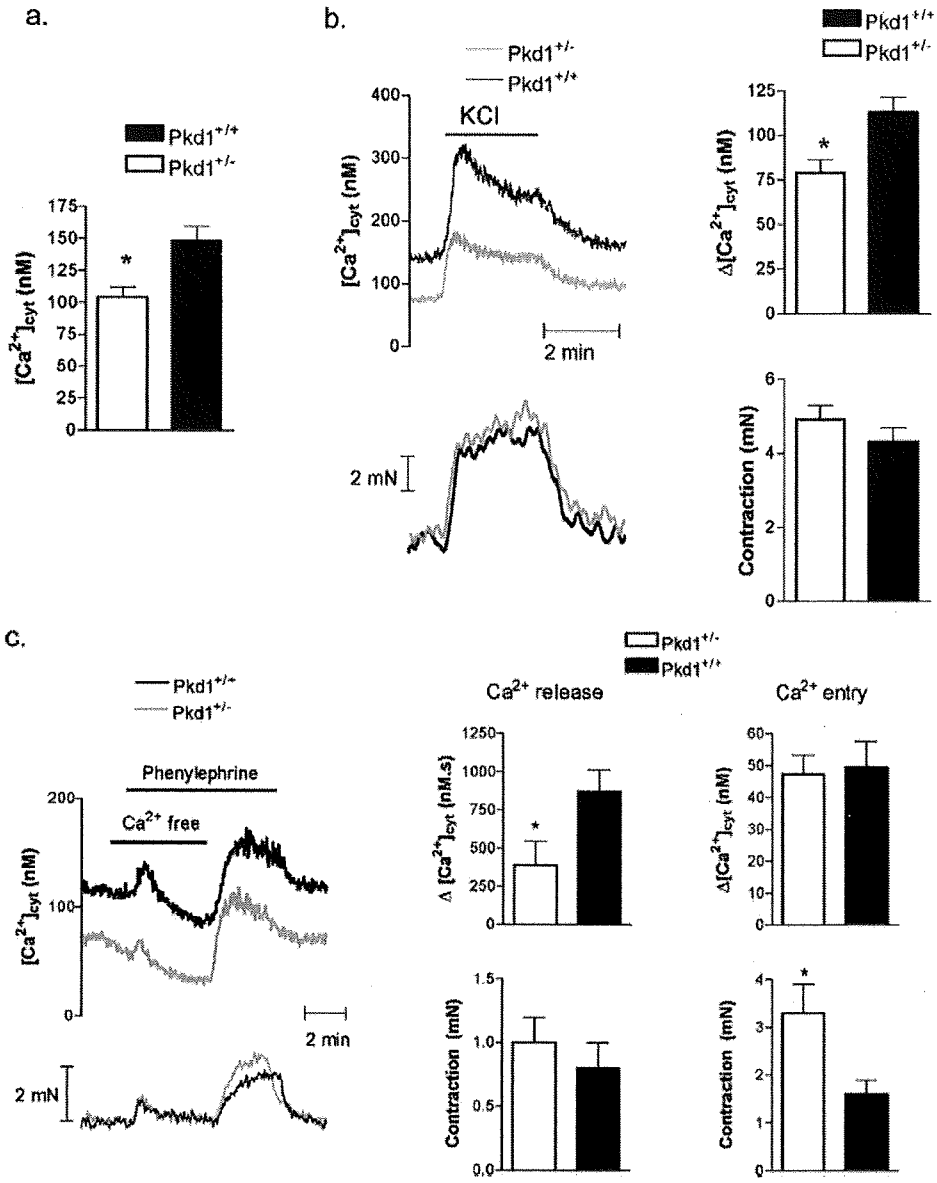

Fig. 2 Cytosolic Ca^{2+} concentration and responses to KCl and phenylephrine in endothelium-denuded aortas isolated from *Pkd1*$^{+/-}$ and *Pkd1*$^{+/+}$. **a** Mean value of cytosolic Ca^{2+} concentration in unstimulated aortic rings from *Pkd1*$^{+/-}$ and *Pkd1*$^{+/+}$ (n=19). **b** Change in cytosolic Ca^{2+} concentration and in contractile tension evoked by 100 mmol/L KCl solution. *Left panel* experimental traces of cytosolic Ca^{2+} concentration (*upper traces*) and contraction (*lower traces*) recorded in aortas from *Pkd1*$^{+/-}$ and *Pkd1*$^{+/+}$. The physiological solution was changed to a 100-mmol/L KCl solution as indicated by the *horizontal bar*. *Right panel* bar graphs showing the mean value of the change in cytosolic Ca^{2+} concentration (*upper graph*) and the contraction (*lower graph*) evoked by the 100-mmol/L KCl solution. Data are the means±SEM from 18 mice. The *asterisk* indicates significant difference between *Pkd1*$^{+/-}$ and *Pkd1*$^{+/+}$ (Student's t test). **c** Effect of phenylephrine on cytosolic Ca^{2+} concentration and contraction in aorta isolated from *Pkd1*$^{+/-}$ and *Pkd1*$^{+/+}$. *Left panel* experimental traces of cytosolic Ca^{2+} concentration (*upper traces*) and contractile tension (*lower traces*) recorded in aorta from *Pkd1*$^{+/-}$ and *Pkd1*$^{+/+}$. Perfusion with Ca^{2+}-free physiological solution and addition of phenylephrine (1 μmol/L) were performed as indicated by the *horizontal bars*. *Right panel* bar graphs showing the mean value of the Ca^{2+} signal (*upper graphs*) and the contraction (*lower graphs*) evoked by phenylephrine in Ca^{2+}-free solution (*left graphs*) or after the readdition of Ca^{2+} into the perfusion solution (*right graphs*). Ca^{2+} release was estimated by the area under the cytosolic Ca^{2+} trace. Data are the means±SEM from eight mice. The *asterisk* indicates significant difference between *Pkd1*$^{+/-}$ and *Pkd1*$^{+/+}$ (Student's t test)

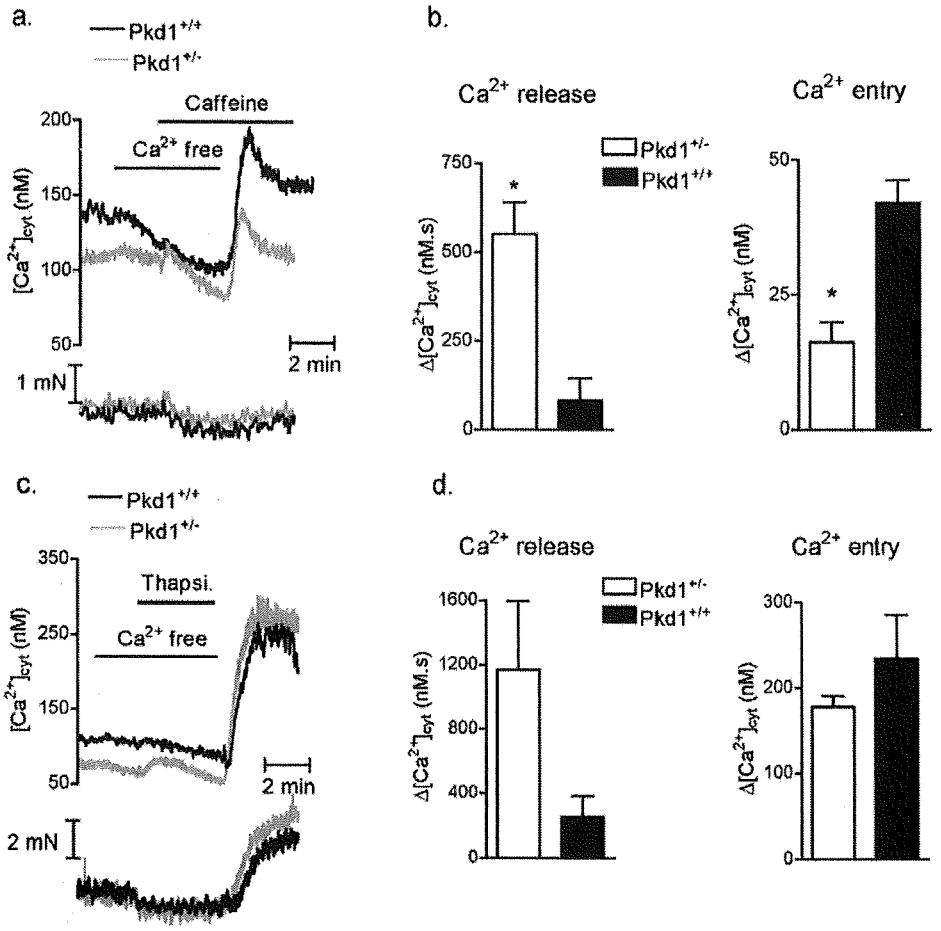

Fig. 3 Intracellular Ca^{2+} release and capacitative Ca^{2+} entry in aorta isolated from *Pkd1*$^{+/-}$ and *Pkd1*$^{+/+}$. **a** Experimental traces of cytosolic Ca^{2+} concentration (*upper traces*) and contractile tension (*lower traces*) recorded in aorta from *Pkd1*$^{+/-}$ and *Pkd1*$^{+/+}$. Perfusion with Ca^{2+}-free physiological solution and addition of caffeine (10 mmol/L) were performed as indicated by the *horizontal bars*. **b** Mean values of the release of intracellular Ca^{2+} evoked by 10 mmol/L caffeine in Ca^{2+}-free solution (*left*) and of the Ca^{2+} entry measured after the readdition of Ca^{2+} into the perfusion solution (*right*). **c** Experimental traces of cytosolic Ca^{2+} concentration (*upper traces*) and contractile tension (*lower traces*) recorded in aorta from *Pkd1*$^{+/-}$ and *Pkd1*$^{+/+}$. Perfusion with Ca^{2+}-free physiological solution and addition of thapsigargin (1 μmol/L) were performed as indicated by the *horizontal bars*. **d** Mean values of the release of intracellular Ca^{2+} evoked by 1 μmol/l thapsigargin in Ca^{2+}-free solution (*left*) and of the Ca^{2+} entry measured after the readdition of Ca^{2+} into the perfusion solution (*right*). Data are the means±SEM from five mice (caffeine) or three mice (thapsigargin). *$P<0.05$, significant difference between *Pkd1*$^{+/-}$ and *Pkd1*$^{+/+}$ (Student's *t* test)

increased in *Pkd1*$^{+/-}$ compared to *Pkd1*$^{+/+}$. The expression of *Orai1* mRNA was significantly lower in *Pkd1*$^{+/-}$ while *Stim1* mRNA level was unchanged. In wild-type aorta, *Serca2a* was fivefold less expressed than *Serca2b*, in agreement with previous report [6]. The level of *Serca2a* expression was significantly enhanced in *Pkd1*$^{+/-}$ aorta vs. *Pkd1*$^{+/+}$, whereas the expression of *Serca2b* was similar. The levels of *eNOS* and *endothelin* mRNA were unchanged. Of note, the *renin* mRNA expression was significantly increased in *Pkd1*$^{+/-}$ kidneys, while *Pkd2* was not different.

Discussion

In this study, we show that reduced *Pkd1* gene dosage in mouse leads to a vascular phenotype characterized by impaired VSM Ca^{2+} homeostasis and age-dependent increased vascular contractility in aorta, which is associated with increased SBP measured in restrained mice and alteration of endothelium-dependent relaxation at age 30 weeks.

Increased vascular contractility was observed in aorta from 20- to 30-week-old *Pkd1*$^{+/-}$ mice, stimulated either with phenylephrine or with the depolarizing KCl solution,

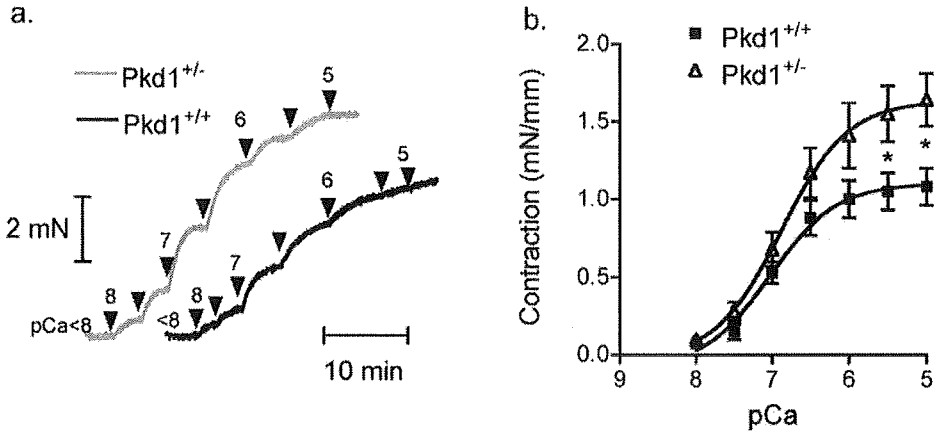

Fig. 4 Ca^{2+}-dependent contraction in ionomycin-permeabilized aorta from $Pkd1^{+/+}$ and $Pkd1^{+/-}$. **a** Typical experimental traces of the contractile tension developed by ionomycin-permeabilized aortic rings from $Pkd1^{+/-}$ and $Pkd1^{+/+}$. Ionomycin-permeabilized aortas were incubated in Ca^{2+}-free solution (pCa<8). Contraction was evoked by cumulatively increasing Ca^{2+} concentration in the bathing solution (pCa 8 to 5, by steps of 0.5 log unit). Ring length: $pkd1^{+/+}$=1.87 mm, $pkd1^{+/-}$=1.78 mm. **b** Mean values±SEM of Ca^{2+}-evoked contraction in ionomycin-permeabilized aortic rings from $Pkd1^{+/-}$ and $Pkd1^{+/+}$ (n= 5). *P<0.05 between $Pkd1^{+/+}$ and $Pkd1^{+/-}$

and was not associated with an increase in the sensitivity to the agonist. This observation is consistent with the increase in contractile response to noradrenaline reported in resistance mesenteric arteries from the Han/SPRD rat model of ADPKD [41] and, recently, in $Pkd2^{+/-}$ mouse arteries [32]. Similarly, the impaired endothelium-dependent relaxation in aorta from 30-week-old $Pkd1^{+/-}$ substantiated the endothelial dysfunction reported in subcutaneous resistance vessels from ADPKD patients [42] and in mesenteric resistance arteries from Han/SPRD rats [41]. These findings, which confirm the previous observation of Muto et al. [23], cannot explain the increased contraction since NOS inhibition did not abolish the difference in contractility observed between $Pkd1^{+/-}$ and $Pkd1^{+/+}$ aortas. Furthermore, q-PCR data indicated that the expression of eNOS was unchanged in $Pkd1^{+/-}$ aortas. Moreover, ex vivo analyses confirmed that angiotensin II produced a larger increase in renal vascular resistance in $Pkd1^{+/-}$ vs. $Pkd1^{+/+}$ mice, whereas the contractile response evoked by NOS inhibition was similar (unpublished data). These observations indicate that increased contractility is neither restricted to α-adrenergic stimulation nor to the aorta.

Two elements suggest that the increased contractility of $Pkd1^{+/-}$ arteries might be caused by an alteration in Ca^{2+} handling. First, the contractile tension is mainly regulated by cytosolic Ca^{2+} concentration; and second, PC1 has been proposed to be involved in Ca^{2+} signaling through its structural interaction with PC2, in such a way that only a normal PC1–PC2 complex is able to function as a Ca^{2+} channel [10]. Our measurements indicated that $Pkd1^{+/-}$ VSMC have a lower resting cytosolic Ca^{2+} than $Pkd1^{+/+}$ cells. Of interest, lower basal cytosolic Ca^{2+} concentration was also detected in the epithelial cells lining the renal collecting ducts from $Pkd1^{+/-}$ mice [1] and in $Pkd2^{+/-}$ VSMC [33]. Taken together, these observations are consistent with the involvement of PC1 and PC2 in Ca^{2+} homeostasis, in both renal epithelial cells and VSMC.

In addition to a low cytosolic calcium level, $Pkd1^{+/-}$ aorta VSMC exhibited several alterations of the Ca^{2+} signal, which could be related to the change in basal calcium or associated with VSMC adaptation to *Pkd1* deficit. Figure 6 summarizes some of the changes that could be involved. Intracellular Ca^{2+} release in response to phenylephrine was significantly decreased in $Pkd1^{+/-}$ aortas. The larger Ca^{2+} release evoked by caffeine or by thapsigargin in $Pkd1^{+/-}$ aortas compared to WT ruled out the possibility of a lower Ca^{2+} content in the SR of $Pkd1^{+/-}$ aortas. Another explanation for the altered phenylephrine response in $Pkd1^{+/-}$ aorta could be the inhibition of the Ca^{2+} release activity of the IP_3 receptor by the lower cytosolic Ca^{2+} [36]. Alternatively, reduced PC1 dosage might impair the process of Ca^{2+} release. PC1 is mainly expressed in the plasma membrane [34] and its interaction with intracellular Ca^{2+} channels has not been reported. However, PC1 associates with PC2 [10, 31], and the latter has been located in the endoplasmic reticulum (ER) [22] where it functions as a Ca^{2+}-activated Ca^{2+} channel [17]. A deficiency in PC1 can cause mislocalization of PC2 from the plasma membrane to the membrane of the ER/SR [10].

The enhanced Ca^{2+} release evoked by caffeine or thapsigargin in $Pkd1^{+/-}$ aorta could reflect an increased uptake of Ca^{2+} into the SR. The q-PCR analyses revealed an increased expression of *Serca2a* mRNA in $Pkd1^{+/-}$ aorta. Of interest, increased VSMC expression of SER-